Pertanika J. Sci. & Technol. 34 (3): 1551 - 1577 (2026)

PERTANIKA JOURNALS

SCIENCE & TECHNOLOGY

Journal homepage: http://www.pertanika.upm.edu.my/

Noise-Resilient and Low Complexity LACO-OFDM Using Approximation Log-Likelihood Ratio (approxLLR) Soft-decision Demodulation with Single-FFT Receiver

Norzalina Othman[1, 3] and Mohd Rashidi Che Beson[2]*

[1]*Faculty of Electronic Engineering and Technology, Universiti Malaysia Perlis (UniMAP), Pauh Putra Campus, 02600 Arau, Perlis, Malaysia*
[2]*Faculty of Intelligent Computing, Universiti Malaysia Perlis (UniMAP), Pauh Putra Campus, 02600 Arau, Perlis, Malaysia*
[3]*Electrical, Electronic and Automation Section (EEA), Universiti Kuala Lumpur Malaysian Spanish Institute (UniKL MSI), Kulim Hi-Tech Park, 09000 Kulim, Kedah, Malaysia*

ABSTRACT

Layered Asymmetrically Clipped Optical Orthogonal Frequency Division Multiplexing (LACO-OFDM) is a promising multicarrier modulation scheme applied in Visible Light Communication (VLC) systems. The conventional LACO-OFDM with iterative receiver introduces high computational complexity and low noise resilience, particularly under high-order modulation and multi-layer configurations. A new enhancement of the demodulation technique based on approximate Log-Likelihood Ratio (approxLLR) with a single-FFT receiver was proposed to address this limitation. The approach enhances noise robustness by estimating bit-wise confidence levels via LLR approximation, while significantly reducing complexity by eliminating the need for pairwise FFT/IFFT operations and the layer-by-layer reconstruction of clipping distortion, which are typically required in conventional LACO-OFDM with iterative receiver demodulation schemes. A significant performance improvement at a target bit error rate (BER) of 10^{-4}, effectively demonstrated with a 4 to 5 times enhancement over the conventional scheme under moderate modulation orders. This corresponds to BER reductions of approximately ~0.705, ~0.615, and ~0.591 orders of magnitude at SNR = 10 dB for 16-QAM, 32-QAM, and 64-QAM. For symbol detection on higher layers (layer≥2), 0.7, 0.3, and 0.1 were identified as optimal scale factors for 4-QAM, 16-QAM, and 64-QAM, respectively. The approxLLR SD approach preserves energy efficiency (EE) in the power analysis, despite only slightly increasing power even with a higher layer count configuration.

Keywords: LACO-OFDM, LLR, optical wireless communication, soft-decision demodulation, visible light communication

ARTICLE INFO

Article history:
Received: 25 September 2025
Accepted: 04 January 2026
Published: 19 June 2026

DOI: https://doi.org/10.47836/pjst.34.3.12

E-mail addresses:
norzalina@unikl.edu.my (Norzalina Othman)
rashidibeson@unimap.edu.my (Mohd Rashidi Che Beson)
* Corresponding author

e-ISSN: 2231-8526

INTRODUCTION

Visible Light Communication (VLC) is a subset of optical wireless communication (OWC) that has emerged as a potential substitute for high-speed data transmission utilising modulated light over unregulated bandwidth. VLC, which operates in the visible light spectrum (380-780 nm; 430-790 THz) (Vappangi et al., 2021; Seow et al., 2021), is a complementary standard of radio frequency (RF) based systems by providing a broader bandwidth, unlicensed channels, low power consumption, immunity to electromagnetic interference, and no health hazards.

VLC research has extensively investigated various areas, including experimental hardware designs, modulation techniques, and applications in diverse environments. Different modulation schemes were designed and developed to meet the varied demands of various applications, including high data rates, energy efficiency (EE), spectral efficiency (SE), bit error rate (BER) performance and system complexity. These aspects have been thoroughly studied in prior research on the VLC system. Orthogonal Frequency Division Multiplexing (OFDM) has evolved as a prominent modulation technique due to its multicarrier structure, which enables data to be transmitted simultaneously over multiple orthogonal subcarriers. This scheme exhibits high spectrum and power efficiency, as well as significant tolerance to inter-symbol interference (ISI) and consistent performance over frequency-selective channels, while maintaining the low complexity of a fundamental framework that enables single-tap signal equalisation (Aliaberi et al., 2019; Jativa et al., 2020; Othman et al., 2024; Vappangi et al., 2021; Zhang et al., 2021).

Extensive research on OFDM-based approaches aimed at optimising the performance of OWC, particularly within the field of VLC technology. Othman et al. (2024) classified OFDM-based modulation into two groups: single-component and multi-component (also known as hybrid-component) OFDM schemes. Single-component OFDM includes Direct Current-biased Optical OFDM (DCO-OFDM), Asymmetrically Clipped Optical OFDM (ACO-OFDM), Pulse-Amplitude Modulated Discrete Multitone (PAM-DMT), Unipolar or Flip OFDM, and enhanced U-OFDM. Meanwhile, Asymmetrically Clipped DC-biased Optical OFDM (ADO-OFDM), Hybrid Asymmetrically Clipped Optical OFDM (HACO-OFDM), Asymmetrically Clipped Absolute-Value Optical OFDM (AAO-OFDM), and Layered ACO-OFDM (LACO-OFDM) were classified as multi-component or hybrid-component OFDM variants (Jativa et al., 2020; Vappangi et al., 2021; Zhang et al., 2021). The OFDM signal or data transmitted via the optical channel must be a real and non-negative signal to comply with the intensity modulation and direct detection (IM/DD) principle.

OFDM modulation is widely utilised in the context of its ability to support high data throughput and strong immunity to ISI. Nevertheless, it inherently suffers from a high peak-to-average power ratio (PAPR), which can limit system efficiency.

To overcome this drawback, modified OFDM schemes such as ACO-OFDM and DCO-OFDM have been introduced. The ACO-OFDM improves BER and PAPR by modulating data on only half of the subcarriers, specifically on the odd subcarriers. Furthermore, DCO-OFDM employs the entire spectrum; however, it suffers from inefficient optical power due to the DC bias required to preserve signal non-negativity (Zhang et al., 2025).

LACO-OFDM was an advancement on ACO-OFDM that improves SE in IM/DD-based communication systems. While maintaining the ACO-OFDM principle, multiple layers of ACO-OFDM symbols were divided and superimposed to exploit more subcarriers without requiring DC bias, thereby improving spectral and power efficiency (Nakano et al., 2023; Zhang et al., 2017;). Despite these advantages, this scheme introduced the incrementation of clipping distortion in the higher layers, which degrades the BER performance. An adaptive modulation and advanced receiver architecture have been developed to address these limitations.

The most recent LACO-OFDM research has focused on improving system efficiency while minimising computational complexity. Adaptive LACO-OFDM, introduced in Nakano et al. (2023), modified the modulation order in each layer dynamically according to the noise level. The needs of the process on multiple layers with different modulation orders result in high computational complexity, which in turn diminishes the practicality of the scheme. Previous studies by Liu et al. (2018) and Zhang et al. (2020) focused on improving LACO-OFDM performance by applying layer precoding and optimal power allocation to strengthen receiver sensitivity and system capacity. Additionally, tone-injection-based PAPR-reduction has been employed to suppress peak signals, hence improve BER performance (Zhang et al., 2017).

Diverse low-complexity approaches have been investigated and studied to address the computational demands of conventional LACO-OFDM with iterative receivers caused by repeated Fast Fourier Transform and Inverse Fast Fourier Transform (FFT/IFFT) operations for symbol reconstruction and clipping distortion (Lowery, 2020). This includes low-complexity LACO-OFDM (L-LACO) using half-size FFT/IFFT operations (Bai et al., 2022), single-FFT receivers (Liu et al., 2020), and single-FFT with pairwise maximum likelihood (ML) detection (Li et al., 2021), all of which offer lower complexity while improving BER performance. Furthermore, the adaptive scheme introduced by Yan et al. (2020) and Zhang et al. (2021) has been devised to improve system performance by adjusting the number of layers (layer count) based on signal-to-noise ratio (SNR) conditions. Collectively, these enhancements demonstrate LACO-OFDM's potential as an efficient and scalable solution for VLC and other OWC systems.

Most of the previous studies on LACO-OFDM have employed hard-decision (HD) demodulation for symbol detection. This modulation maps the received symbols directly to the nearest constellation points, resulting in inferior performance under noisy conditions.

Soft-decision (SD) demodulation improves detection reliability by utilising log-likelihood ratios (LLRs) to quantify bit-wise confidence, leading to an increase in BER performance, particularly with high-order modulation schemes. However, the complexity of the full exact LLR computation exponentially increases with high-order modulation, requiring the simpler scheme development.

Olivatto et al. (2017) proposed Simplified LLR demappers for high-order Phase-Shift Keying (PSK) and Amplitude and PSK (APSK) that substantially reduce complexity with no performance loss as compared to the Max-Log-MAP (Maximum a Posteriori) soft-demapper. Meanwhile, Mao et al. (2020) improved a simplified LLR soft demodulation algorithm for 64-QAM, which optimises decision rules to decrease computational complexity while minimising performance loss significantly. However, its effectiveness may be limited when applied to different modulation orders without further modifications. Another study investigated the integration of SD approaches into system-level designs, utilising LLR-assisted Viterbi decoders (Wang et al., 2023), which improve BER performance yet face the constraint length as a constraint.

The implementation of long irregular low-density parity-check (LDPC) codes in SD decoding has demonstrated considerable BER improvements and coding advantages over HD decoding, particularly in high-order QAM applications. This makes SD decoding well-suited to high-capacity optical communication, as reported by Hussein et al. (2021), which exhibits improved system performance while highlighting the importance of implementations that balance performance gains with computational efficiency.

A simplified LLR applied in OFDM with index modulation (OFDM-IM) as presented by Hu et al. (2018), utilises an SNR-dependent radius to identify the number of most likely transmitted symbols. OFDM-IM thereby reducing computational complexity while attaining near-optimal BER performance. The integration of index modulation and bandwidth optimisation in LACO-OFDM demonstrates a significant enhancement in SE and robustness across different channel conditions (Azim et al., 2021). In other related development, Anand et al. (2024) introduced a simplified LLR detector for OFDM systems based on the fractional Fourier transform (FrFT), which notably mitigates intercarrier interference (ICI) typically encountered in conventional intensity modulation OFDM (IM-OFDM) configurations.

Despite LACO-OFDM's promising performance in improving SE, current receiver architectures are computationally intensive. Conventional LACO-OFDM receivers commonly rely on pairwise FFT/IFFT processing for symbol reconstruction and clipping distortion, which incur significant complexity as the number of layers and modulation order increase. Several low-complexity single-FFT receivers have been reported; however, these approaches predominantly adopt HD demodulation that does not exploit bit-wise reliability information. Moreover, existing LLR demodulation techniques are generally developed

for general optical OFDM and do not explicitly account for the layer-dependent clipping noise inherent in LACO-OFDM systems.

To the best of the authors' knowledge, a LACO-OFDM framework that integrates a bit-wise LLR-based SD demodulation with a single-FFT receiver while preserving robustness against clipping distortion has not been previously reported. This work addresses this gap as well as mitigates a drawback encountered by conventional LACO-OFDM with an iterative receiver by proposing a new enhancement approach of LACO-OFDM that incorporates a noise-resilient, low-complexity demodulation scheme as presented in this research article. This enhanced version of LACO-OFDM uses an approximate LLR (approxLLR) SD demodulation with a single-FFT receiver configuration. A layer-by-layer SD framework has been adopted, aimed at enhancing both BER performance and SE. Computational efficiency is achieved by eliminating the need for the pairwise FFT/IFFT operation typically used for symbol reconstruction and clipping distortion suppression as implemented in Lowery (2020). Instead, higher-layer symbols are efficiently detected through direct subtraction of the received symbol from its corresponding modulation reference. Furthermore, the approxLLR preserves bit-level reliability by estimating the likelihoods, mapping probability values to the bit representations, and selecting the most probable symbol for final decoding.

The remaining sections of the article are organised as follows: the proposed modulation scheme is outlined in the Methodology section. Section Results and Discussion present the results and performance evaluation of the LACO-OFDM approxLLR SD demodulation with a single-FFT receiver in comparison to the conventional LACO-OFDM with an iterative receiver scheme. The conclusion section concludes with a summary of the research findings, the implications of the research work and the practical relevance of the proposed approach.

METHODOLOGY

This section presents the proposed LACO-OFDM using approxLLR SD demodulation with a single-FFT receiver applied in a VLC link. It begins with an overview of conventional ACO-OFDM and LACO-OFDM principles, followed by a detailed mathematical model of the transmitter and receiver of the proposed approach. Finally, simulation outcomes of the proposed approach are evaluated and compared with the conventional LACO-OFDM with an iterative receiver scheme using performance analysis formulae as discussed in this section to completely examine the proposed approach's effectiveness and improvements.

ACO-OFDM and LACO-OFDM Principle

ACO-OFDM exploits the signal's anti-symmetry and clipped at zero on the negative values to achieve non-negativity without losing information. The system's design ensures that any distortion caused by clipping only applies to subcarriers that do not carry data,

which occurs on even subcarriers, allowing the receiver to accurately detect symbols on odd subcarriers. This approach is highly beneficial in optical communication to ensure the reliability of transmitted data while fulfilling the requirements of VLC systems.

Conventional ACO-OFDM loads data solely on odd subcarriers, leaving even subcarriers unoccupied. The constellation mapping, Serial to Parallel (SP), Hermitian Symmetry (HS), Inverse Fast Fourier Transform (IFFT), Parallel to Serial (PS), zero clipping and Cyclic Prefix (CP) were imposed in the transmitter, while CP removal, Fast Fourier Transform (FFT) and de-mapping were imposed in the receiver. Despite this method being spectrally efficient, the amount of data it can transmit in each bandwidth is limited. To address this issue, multiple L layers ACO-OFDM modulated symbol on several N Subcarriers were stacked or superimposed to create LACO-OFDM.

Equation 1 defines the number of occupied subcarriers in layered ACO-OFDM N_L can be represented by:

$$N_L = \sum_{l=1}^{L} \frac{N}{2^l} \quad [1]$$

with the maximum number of layers L provided by Equation 2 can be calculated as:

$$L = \log_2 N - 1 \quad [2]$$

However, the commonly applied number of layers is between 4 or 5 layers as reported in Zhang et al. (2019), sufficient to strike the trade-off between throughput and energy consumption.

Each layer's anti-symmetry allows clipping without losing data, and the successive demodulation scheme enables the receiver to independently retrieve data from each layer. Due to the layered approach, which maximises data transmission within a specified bandwidth, LACO-OFDM is adequate for high-speed VLC systems.

In traditional LACO-OFDM with L layers and N Subcarriers, the input data is first mapped to QAM symbols, then HS is applied to the subcarriers to ensure that the signal is real-valued in the time domain. Only the odd subcarriers carry data, resulting in an anti-symmetric time domain after the IFFT, represented by Equation 3 as the frequency domain of the symbol vector X_k :

$$X_k = \left[0, X_1, 0, X_3, \dots, X_{\frac{N}{2}-1}, \dots, X^*_{\frac{N}{2}-1}, \dots, , X^*_3, 0^*, X^*_1\right], k = 0, 1, 2, \dots, \frac{N}{2} - 1 \quad [3]$$

where X_k denotes the M-QAM symbol of k-th subcarrier index and $(.)^*$ denotes complex conjugate after performing HS computation. In the l-th layer, the constellation symbols are assigned to subcarriers with index given by $2_{l(2k+1)}2^{l-1}(2k+1)$ where $k = 0,1,2,\ldots,\frac{N}{2^l}-1$. All other subcarriers are set to zero.

To meet the non-negativity constraint, the negative components of x_n demonstrate by Equation 4 as time domain data symbol, are clipped to zero, resulting in x_{zclip} on the n-th element. The CP computation is then performed for each layer l and is defined as:

$$x_n^{(l)} = \frac{1}{2}\, x_n^{(l)} + x_{zclip}^{(l)}\ , n = 0, 1, 2, \ldots, N-1 \qquad [4]$$

After the CP computational, all symbol in L layer is superimposed and the superimposed symbol represent by $x_{LACO,n}$ before being transmitted to optical channel. The received LACO-OFDM symbols denoted by Equation 5 as:

$$y_n = x_{LACO,n} * h_n + w_n \qquad [5]$$

where:

y_n: received signal

$x_{LACO,n}$: superimposed transmit signal

h_n: channel impulse response

w_n: Additive white Gaussian noise (AWGN)

Note. Shot noise and thermal noise are well modelled as AWGN (Bai et al., 2022)

As in the receiver, after the CP removal and FFT computation, the ACO-OFDM symbol can be detected layer by layer using Equation 6 by employing clipping distortion subtraction to obtain a new received frequency domain of $\hat{R}_k^{(l)}$:

$$\hat{R}_k^{(l)} = \arg min_{X \in S} \left| X - 2\hat{R}_k^{(l-1)} \right|, \qquad \text{k= 1, 3, 5, ….,} \frac{N}{2} - 1 \qquad [6]$$

where:

S : constellation set mapping of X symbol

$\hat{R}_k^{(l-1)}$: received frequency-domain symbol of the previous layer

LACO-OFDM Transmitter

Figure 1 shows the proposed LACO-OFDM transmitter by adding a layer occupied the ACO-OFDM principle. The input data stream is first mapped onto a complex frequency-domain symbol X_{CQAM}, where $CQAM = 1,2,3,\dots,N$ based on the given M-QAM constellation before being split into L parallel layer division for the layer number of l-th as denoted by Equation 7.

$$X^{l}_{2^{l-1}(2k+1)}, \quad k = 0,1,2,\dots,\frac{N}{2^{l}} - 1 \qquad [7]$$

To generate a real-value of time-domain symbol as indicate in Equation 8, HS is imposed on the symbol in the odd subcarrier by setting the first index and $\frac{N}{2}$ index to zero as :

$$X^{l}_{k} = \begin{cases} X^{l}_{k} = X^{*l}_{N-k}, \quad k = 0,1,2,\dots,\frac{N}{2} - 1 \\ X^{l}_{0} = 0 \\ X^{l}_{\frac{N}{2}} = 0 \end{cases} \qquad [8]$$

where (*) denotes the conjugate of complex numbers.

For example, the active symbol in the layer $l = 1$ demonstrate in Equation 9 is represented as follows:

$$X^{1} = \left[0, X_1, 0, X_3, \dots, 0, X_{\frac{N}{2}-1}, 0, X^{*}_{\frac{N}{2}-1}, \dots, , X^{*}_{3}, 0^{*}, X^{*}_{1}, 0\right] \qquad [9]$$

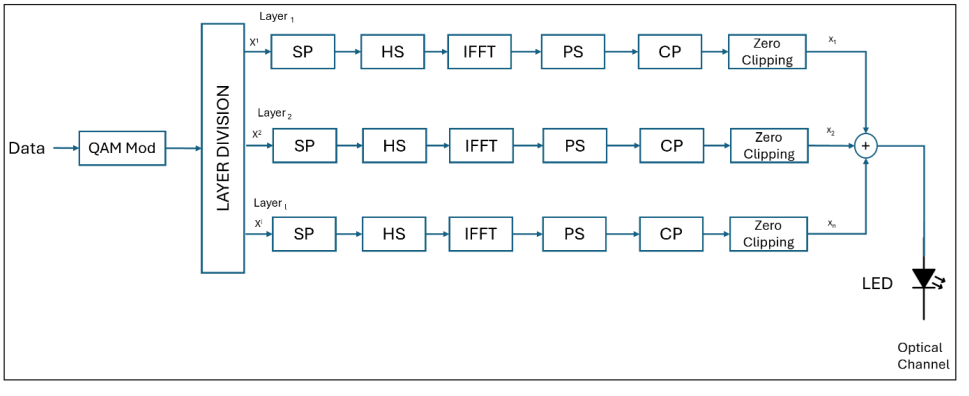

Figure 1. LACO-OFDM approxLLR SD transmitter block diagram

Equation 10 defines the time-domain signal of the layer l-th, x_n^l were obtained after N-point of IFFT, becomes real-valued and anti-symmetric by performing the following equation:

$$x_n^l = \frac{1}{\sqrt{N}} \sum_{k=0}^{N-1} X_k^{(1)} \; exp\left(j \frac{2\pi}{N} nk\right), n = 0,1,2,3, \dots, N \quad [10]$$

which follows a half-wave symmetry provide by Equation 11 as:

$$x_n = x_{n+\frac{N}{2}}, \quad n = 0,1,2,3, \dots, \frac{N}{2} - 1 \quad [11]$$

Hence, the negative time-domain symbol that commonly falls or appears at the even subcarrier can be clipped to zero, $\lfloor x_n^l \rfloor_{zclip}$ as define in Equation 12 without any loss of information.

$$\lfloor x_n^l \rfloor_{zclip} = \begin{cases} x_n^l, & x_n^l \geq 0, \\ 0, & x_n^l < 0 \end{cases} \quad [12]$$

The distortion caused by clipping is compensated for by adding $\frac{1}{4}\ N$ CP to mitigate inter-layer interference (ILI) and ISI.

In the layered ACO-OFDM transmitter, different layers are superimposed in the time domain and written as in Equation 13:

$$x_{LACO,n} = \sum_{l=1}^{L} \lfloor x_n^l \rfloor_{zclip}, \quad n = 0,1,2,3, \dots, N-1 \quad [13]$$

where:

$x_{LACO,n}$ – superimposed time-domain symbol

L – total number of layers of LACO-OFDM

$\lfloor x_n^l \rfloor_{zclip}$ – time-domain zero clipping symbol of the layer l

Lower clipping of the time-domain signal will generate distortion in the frequency domain. Since the effects only fall on even subcarriers in every layer, only the signal of the layer $l \geq 2$ are distorted. The distorted result from the lower layer has been added in the frequency-domain symbol as illustrated in Figure 2.

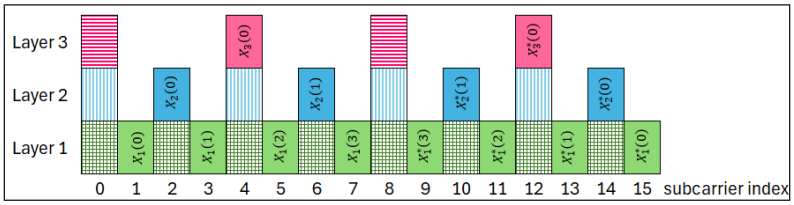

Figure 2. 3-layer ACO-OFDM with 16-point FFT in frequency domain view to illustrate the superimposed layers
Note. (*) It is a symbol of Hermitian symmetry conjugate

Proposed LACO-OFDM Approximate LLR Soft-Decision Algorithm with Single-FFT Receiver

The previous study conducted by Bai et al. (2022) and Cao et al. (2019) imposed an iterative receiver with a subtraction operation of clipping distortion, which is done layer by layer (successive detection). The symbols in the higher layer are recovered after the negative clipping distortion from the corresponding layer has been removed. Even though this approach offered high SE, it faced computational complexity issues.

Figure 3 shows a block diagram of the proposed LACO-OFDM receiver. In this study, an approxLLR is employed in SD demodulation. Then, the approxLLR values of $q = \log_2(M)$ bits of symbol R_k^l are estimated to calculate the bit probabilities of all bits in the symbol. The following paragraph includes a comprehensive explanation regarding the proposed method.

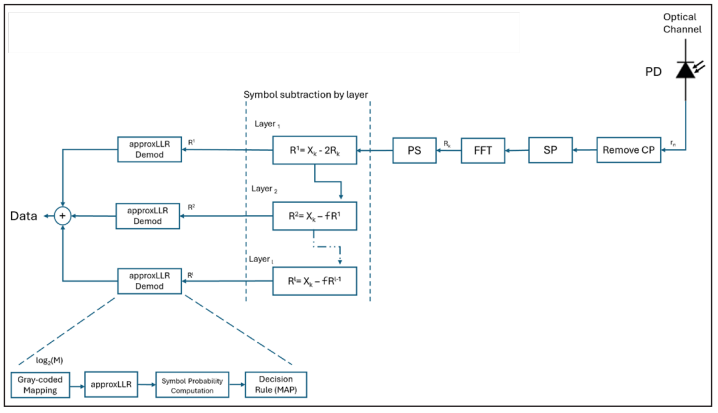

Figure 3. LACO-OFDM approxLLR SD with single-FFT receiver block diagram

For l- In the layer ACO-OFDM, the CP removal is imposed on the received time-domain symbol, r_n and FFT computation was applied to generate the frequency-domain symbol, R_k and represented by Equation 14 as:

$$R_k = \frac{1}{\sqrt{N}} \sum_{n=1}^{N} r_n \, exp\left(j \, \frac{2\pi}{N} nk\right), \quad k = 0,1,2,3, \ldots, \frac{N}{2} - 1 \qquad [14]$$

The first layer $l = 1$ is free from ILI, whereas all subsequent layers are affected by ILI from the preceding layers, ranging from layer $l = 1$ to L. For $l = 1$, the transmitted symbol could be directly detected by using an odd subcarrier of $R_k = R_k^1$ and denoted in Equation 15 by:

$$\hat{R}_k^1 = argmin_{X \in CQAM} \left| X_k - 2R_k^1 \right| \;, k = 1,3,5, \ldots, \frac{N}{2^l} \qquad [15]$$

where $CQAM$ represent the complex number of the constellation set of X symbol and the scale factor of 2 in Equation 15 is because the clipping operation reduces the power of ACO-OFDM symbols in the odd subcarriers by half (Wang et al., 2015).

For the subsequent layer, $l = 2$ to L, the transmitted symbol can be detected using Equation 16 by:

$$\hat{R}_k^l = argmin_{X \in CQAM} \left| X_k - f\hat{R}_k^{(l-1)} \right| \qquad [16]$$

where:

$\hat{R}_k^{(l-1)}$ = received frequency-domain symbol of the previous layer

$k = 1(2^{(l-1)}),3(2^{(l-1)}),5(2^{(l-1)}), \ldots, \frac{N}{2^l}(2^{(l-1)})$

f = scale factor

Figure 4 illustrates the sequential operations executed within the approxLLR demodulation block. Specifically, the diagram presents a step-by-step representation of how the received frequency-domain symbols are decoded, starting with the mapping of the noisy received symbols onto the M-ary QAM constellation, followed by the evaluation of Euclidean distances between the received symbols and candidate constellation points.

These distances are then used to approximate the bit-wise log-likelihood ratios, producing a soft-decision output for each bit position associated with a symbol. A Maximum a Posteriori (MAP) decision rule is applied to select the most probable transmitted symbol, enabling accurate symbol recovery under noise and interference conditions.

Initially, the received frequency-domain symbol $\hat{R}_k^l$ undergoes Grey-coded mapping onto the M-QAM constellation. This process is carried out after subtracting the interference introduced by the preceding layer, as described in the previous step in Equation 16. The use of Grey-coded mapping ensures that each symbol is represented by its corresponding bit sequence in such a way that adjacent constellation points differ by only a single bit, thereby reducing the likelihood of bit errors during demodulation. Each mapped symbol in the constellation can be expressed as a binary vector as described in Equation 17.

Let the constellation size be M, the number of bits per symbol is represented as $q = \log_2(M)$. For the i-th received symbol, the associated bit vector is defined as:

$$b_i = \left[b_{i,1}, b_{i,2}, \ldots, b_{i,q}\right], \; b \in \{0,1\}^q \qquad [17]$$

Figure 5 is the illustration of a 16-QAM constellation with Gray-coded mapping with bit label format $[b_1\ b_2 \mid b_3\ b_4]$ with last-MSB order where:

b_1b_2 = Grey-coded bits for the I-axis (In-phase).

b_3b_4 = Grey-coded bits for the Q-axis (Quadrature).

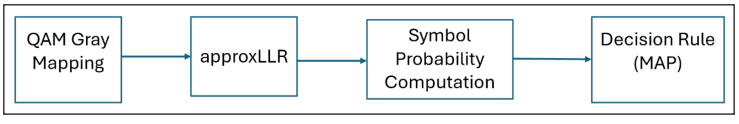

Figure 4. ApproxLLR SD demodulation block diagram

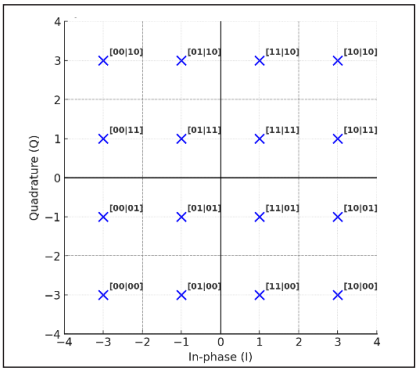

Figure 5. 16-QAM constellation with Gray-coded bit label $[b_1\ b_2 \mid b_3\ b_4]$

To recover these bits at the receiver, each bit is split into 2 subsets, $S_q^{(0)}$ *or* $S_q^{(1)}$ and subsequently the demapper computes approxLLR using Euclidean distance of 1-D nearest squared distance between the binary vector of $b_{i,q}$ and constellation point.

Figure 6 illustrates the 16-QAM constellation diagram, with the in-phase (I) and quadrature (Q) axes defined by the discrete amplitude levels {−3d, −d, +d, +3d}. These levels correspond directly to the 1-D Grey-coded mapping of 16-QAM. The constellation points are explicitly labelled along each axis according to the governing Equation 18:

$$\mathcal{A} = \left\{ \pm(2i-1)d \mid i = 1,2,\ldots,\frac{\sqrt{M}}{2} \right\} \quad [18]$$

where:

$\mathcal{A}$ – Axis level

d - spacing parameter (half of the step between adjacent levels)

i- index (1 to $\frac{\sqrt{M}}{2}$) that generates the inner to outer levels

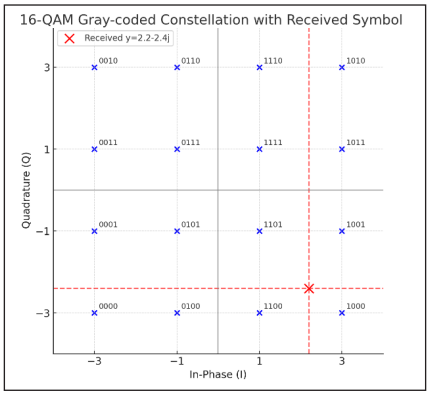

Figure 6. 16-QAM Gray-coded constellation with received bit

Specifically, for the i-th received symbol, the approxLLR corresponding to the q-th bit position in Equation 19 is given by:

$$\mathcal{L}_{i,q} \approx \frac{min_{s \in S_q^{(0)}} |y_i - s|^2 - min_{s \in S_q^{(1)}} |y_i - s|^2}{\sigma^2} \quad [19]$$

where:

$S_q^{(0)}$ – subset of constellation points with bit $b_q = 0$

$S_q^{(1)}$ – subset of constellation points with bit $b_q = 1$

y_i – received symbol after grey-coded mapping demodulation

σ^2 – noise variance of thermal and shot noise (AWGN)

From Equation 19, $\mathcal{L}_{i,q}$ denotes the LLR associated with q-th bit of the i-th received symbol, quantifies the relative likelihood of bit either 1 or 0, which stores the LLR values of all N grey-mapped received symbol across all bit positions in the LLR matrix $\left[\mathcal{L}_{i,q}\right]_{\substack{i=1,\ldots,N \\ q=1,..,\log_2 M}}$. Subsequently, a probability score is assigned for every candidate of a symbol $m \in \{0, 1, \ldots, M-1\}$ by computing the product of the bitwise posterior probability shown in Equation 20, represented by:

$$\tilde{P}_m^{(i)} \propto \prod_{q=1}^{\log_2(M)} P\left(b_q = b_{m,q} | y_i\right) \qquad [20]$$

with each posterior derived directly from the LLR value demonstrate by Equation 21 as:

$$P\left(b_{i,q} = b | y_i\right) = \begin{cases} \frac{e^{\mathcal{L}_{i,q}}}{1+e^{\mathcal{L}_{i,q}}} & , \quad b = 0 \\ \frac{1}{1+e^{\mathcal{L}_{i,q}}} & , \quad b = 1 \end{cases} \qquad \text{where } b \in \{0,1\} \qquad [21]$$

This operation produces an unnormalised likelihood score for every candidate symbol. Finally, the maximum a posteriori (MAP) criterion is applied to identify the most likely transmitted symbol. Equation 22 provides estimated symbol index $\hat{m}^{(i)}$ is obtained by:

$$\hat{m}^{(i)} = \arg max_{m \in \{0,1,\ldots,M-1\}} \tilde{P}_m^{(i)} \qquad [22]$$

By repeating this operation for all received symbols, the final output sequence is $\hat{s} = \left[\hat{m}^{(1)}, \hat{m}^{(2)}, \ldots, \hat{m}^{(N)}\right]$, which constitutes the estimated transmitted symbol stream.

The performance of the proposed approxLLR SD demodulation with a single-FFT approach for the LACO-OFDM system is evaluated through a detailed analysis of the BER and the received power signal. The BER is computed by comparing the detected mismatched bits between the transmitted sequence x_i with the detected received sequence y_i and denoted in Equation 23 Equation 23 for M-QAM over an AWGN channel.

$$BER = \frac{1}{N}\sum_{i=1}^{N}[x_i - y_i] \quad [23]$$

The received power as shown in Equation 24 is estimated after adding AWGN noise and is denoted as:

$$P_{rx} = \frac{1}{N}\sum_{n=1}^{N}|y[n]|^2 = P_{signal} + \sigma^2 \quad [24]$$

where:

P_{rx} : Received power

$y[n]$: received signal after channel noise

N: total number of signal samples

σ^2 : noise variance

The BER performance analysis of both approaches can be calculated by using the order of magnitude difference (OMD) represented by Equation 25:

$$OMD = \log_{10}\frac{BER^{(iter)}}{BER^{(sfft)}} \quad [25]$$

where:

OMD – order of magnitude difference

$BER^{(iter)}$ – BER of conventional iterative- receiver HD at specific SNR

$BER^{(sfft)}$ - BER of single-FFT receiver SD at specific SNR

RESULT AND DISCUSSION

A MATLAB simulation was performed to evaluate the performance of a conventional LACO-OFDM system employing HD demodulation compared to the proposed LACO-OFDM approxLLR with a single-FFT receiver system utilising an SD scheme. Table 1 summarises the parameters employed in the subsequent simulation outcome.

Table 1
Simulation parameter

Description	Parameter
Symbol length (m)	512
No. of subcarriers (N)	1024
Data size	m × N
No of Layer (***L***)	2/3/4
QAM Mod order (M)	4/16/32/64
IFFT size	N-point
FFT size	$\frac{N}{2}$ point
No. of Cyclic Prefix (Ncp) size	$\frac{1}{4} \times N$

Computational Complexity

This section presents a computational complexity analysis of the conventional LACO-OFDM with iterative receiver employing HD demodulation and the proposed approxLLR SD with single-FFT receiver approach, both applied within the LACO-OFDM framework. The complexity evaluation is based on the number of complex-valued multiplications required for the FFT/IFFT operations involved in clipping distortion estimation of the symbol reconstruction-subtraction operations performed at each layer. The complexity of the demapper type approach is also discussed in this section.

The conventional LACO-OFDM with iterative receiver utilising HD demodulation requires pairwise FFT/IFFT with two $\frac{N}{2}$-point FFT and one N-point IFFT operations to regenerate the frequency-domain clipping distortion for each layer of the ACO-OFDM signal. This repeated transformation process significantly contributes to the overall computational complexity. The complexity associated with the N-point IFFT and $\frac{N}{2}$-point FFT operations are denoted in Equation 26 as:

$$IFFT = \mathcal{O}\ (N\ log_2 N\ )$$
$$FFT = \mathcal{O}\left(\frac{N}{2}\ log_2 N\right) \quad [26]$$

The complexity of conventional LACO-OFDM with iterative receiver HD, as denoted in Zhang et al. (2021), can be represented in Equation 27 as:

$$\begin{aligned} \mathcal{O}_{convHD} &= \mathcal{O}(N\ log_2 N) + 2\,\mathcal{O}\left(\frac{N}{2} log_2 N\right) \\ &= \mathcal{O}(N\ log_2 N) + \mathcal{O}(N\ log_2 N) \\ &= 2\mathcal{O}(N\ log_2 N) \end{aligned} \quad [27]$$

For the L – layer of LACO-OFDM, the conventional LACO-OFDM with iterative receiver HD performs layer-by-layer reconstruction and subtraction, iteratively and is presented in Liu et al. (2020) using Equation 28 as:

$$\begin{aligned} \mathcal{O}_{ConvHD} &= L\,.\left(\mathcal{O}(N\ log_2 N) + 2\mathcal{O}\left(\frac{N}{2} log_2 N\right)\right) \\ &= L\,.2\,.\mathcal{O}(N\ log_2 N) \\ &= L2\mathcal{O}(N\ log_2 N) \end{aligned} \quad [28]$$

In HD QAM demodulation, no multiplication or distance computation is required, as it is based on a quantisation decision. Hence, the demapper complexity of HD demodulation per symbol is $\mathcal{O}(1)$. The direct threshold comparison is imposed on every symbol across all layers, with the total number of symbols, N_s as indicate in Equation 29 by:

$$N_s = \frac{N}{2}\left(1 - \frac{1}{2^L}\right) \quad [29]$$

In contrast, the proposed approxLLR SD demodulation utilises a single-FFT receiver, requiring only one N-point FFT operation at the receiver. The associated computational complexity for L – layer LACO-OFDM is represented by Equation 30 as:

$$\mathcal{O}_{Single\ -FFT} = \mathcal{O}(N\ log_2 N) \quad [30]$$

This demonstrates that the approxLLR SD with the single-FFT approach reduces computational complexity by a factor of approximately 2 times compared to the conventional LACO-OFDM with iterative-receiver HD scheme. Such efficiency is particularly beneficial for real-time VLC systems, where low latency and minimal processing time are critical requirements.

The proposed approach is imposed with a bit-wise demodulation operation, and the complexity of approxLLR computation across all layers of L denoted in Equation 31 as:

$$\mathcal{O}_{approxLLR} = \mathcal{O}(N\ log_2 N) + \frac{N}{2}\left(1 - \frac{1}{2^L}\right) \cdot \mathcal{O}\left(q\sqrt{M}\right), \quad [31]$$

where $q = log_2 M$

The demapper complexity of approxLLR $\mathcal{O}\left(q\sqrt{M}\right)$ derive from the arithmetic operation (addition, subtraction, multiplication and comparison) involved in distance calculation, bit-wise minimum selection and scaling computation (refer to Equation 19). By computing a 1-D nearest squared distance on metrics of $t = \sqrt{M}$ amplitude levels in-phase (I) and quadrature (Q) components separately, the computation required $2t$ real subtraction and $2t$ real multiplication for detected subcarriers. The subsequent bitwise LLR computation involves selecting two minima matrices per bit from a subset of size $\frac{t}{2}$ where require $\left(\frac{t}{2} - 1\right)$ comparison. Thus, the required minima comparison per bit is denoted in Equation 32 as:

$$\left(\frac{t}{2} - 1\right) + \left(\frac{t}{2} - 1\right) = t - 2 \quad [32]$$

resulting in $q(t-2)$ comparison across all q bits followed by $1q$ single subtraction and $1q$ single scaling operation per bit.

The final complexity per detected subcarrier of approxLLR demodulation in Equation 33 is summarised by:

$$\begin{aligned} N_{sub} &= 2t + q \quad \text{- subtraction operation of } N \text{ subcarrier} \\ N_{mul} &= 2t + q \quad \text{- multiplication operation of } N \text{ subcarrier} \\ N_{cpr} &= q(t-2) \quad \text{- comparison operation of } N \text{ subcarrier} \end{aligned} \quad [33]$$

The overall approxLLR demodulation complexity $\mathcal{O}\left(q\sqrt{M}\right)$ is derive by $T_{approxLLR}$ summation of operations in Equation 33 makes it the total arithmetic cost per subcarrier denotes in Equation 34 as:

$$\begin{aligned} T_{approxLLR}\ (M) &= N_{sub} + N_{mul} + N_{cpr} \\ &= (2t+q) + (2t+q) + q(t-2) \\ &= t(q+4) \end{aligned} \quad [34]$$

Since multiplying a constant does not change the growth in Big-O $(\mathcal{O})$ analysis and the constant multipliers are omitted, therefore $T_{approxLLR}\ (M) = \mathcal{O}(qt)$ and substitute $t = \sqrt{M}$, then the approxLLR demodulation computation shown in Equation 35 is represented as:

$$T_{approxLLR}\ (M) = \mathcal{O}\left(q\sqrt{M}\right) \quad [35]$$

The most likely transmitted symbol is then obtained with a MAP decision on the LLR symbols, which incurs only $\mathcal{O}(1)$ operation, therefore, the combined demapping and symbol identification complexity remains $\mathcal{O}\left(q\sqrt{M}\right)$.

The approxLLR demappers overhead, combined with the single-FFT receiver architecture, contributes to a favourable complexity–performance trade-off while preserving the benefits of soft-decision demodulation. The complexity remains scalable and efficient, especially when using moderate modulation orders and layers. A comparative summary of conventional LACO-OFDM with iterative-receiver HD versus approxLLR SD with single-FFT receiver complexity is present in Table 2.

Table 2
Comparative summary

Component	Iterative-receiver HD	approxLLR SD with Single-FFT
IFFT/ FFT Complexity	$L2\mathcal{O}(N\ \log_2 N)$	$\mathcal{O}(N\ \log_2 N)$
Demapper Complexity	$\frac{\mathrm{N}}{2}\left(1-\frac{1}{2^{\mathrm{L}}}\right)\cdot\mathcal{O}(1)$	$\frac{\mathrm{N}}{2}\left(1-\frac{1}{2^{\mathrm{L}}}\right)\cdot\mathcal{O}\left(q\sqrt{M}\right)$
Total Complexity	$\mathcal{O}_{ConvHD} = L2\mathcal{O}(N\ \log_2 N) + \frac{\mathrm{N}}{2}\left(1-\frac{1}{2^{\mathrm{L}}}\right)\cdot\mathcal{O}(1)$	$\mathcal{O}_{approxLLR} = \mathcal{O}(N\ \log_2 N) + \frac{\mathrm{N}}{2}\left(1-\frac{1}{2^{\mathrm{L}}}\right)\cdot\mathcal{O}\left(q\sqrt{M}\right)$

Numerical Result

Figure 7 compares the conventional LACO-OFDM with iterative receiver against the proposed LACO-OFDM approxLLR SD with single-FFT receiver across varying QAM orders. At an SNR of 10 dB, the proposed method achieves performance gains of approximately 5×, 4×, and 3.9×, where × represents times, over HD demodulation for 16-QAM, 32-QAM, and 64-QAM, corresponding to order-of-magnitude reductions of 0.705, 0.615, and 0.591, respectively. Conversely, for 4-QAM, the method underperforms, yielding an improvement ratio of just 0.133 (≈ -0.877 order of magnitude). These findings indicate the effectiveness of the proposed approxLLR SD demodulation, which derives bit-wise likelihoods via probabilistic estimation rather than conventional map to the nearest-neighbour decisions performed by HD demodulation, which makes it more susceptible to noise-induced errors. By incorporating bit-wise likelihood information, the SD process can refine the estimation of each transmitted symbol with higher accuracy. The receiver is allowed to differentiate more effectively between closely spaced constellation points, particularly under noisy optical channel conditions. As illustrated in Figure 7, the proposed approach yields a performance gain of approximately ~4dB at a BER of 10^{-4} and about ~3dB at 10^{-5} for 64-QAM. These improvements demonstrate the robustness and efficiency of higher-order QAM formats.

Figure 8 depicts the BER performance of the proposed approach for various M-QAM modulation schemes, 4-QAM, 16-QAM, 32-QAM, and 64-QAM. The results show that 4-QAM has significant noise tolerance, sustaining a continuously low BER under relatively low SNR conditions. The observation demonstrates the practicality of the proposed approach by preserving transmission reliability even in high-noisy conditions. For comparison, 16-QAM and 32-QAM generally achieve a reasonable balance (trade-off) between SE and noise resistance, although they require higher SNR values to maintain acceptable BER performance. While 64-QAM, despite offering the highest SE, exhibits greater vulnerability to noise and demands a substantially higher SNR to ensure reliable data transmission. This sensitivity becomes more evident in LACO-OFDM structures, where asymmetric zero-clipping and superimposed layers introduce additional distortion to the received symbols. The result reinforces the fundamental trade-off in QAM modulation order: lower-order are more reliable in low-SNR, whereas higher-order modulation is suited for delivering high data rates under favourable signal conditions. Thus, selecting the right modulation order is crucial in attaining the optimal balance of SE and error performance.

Figure 9 presents the BER performance of the proposed approach on various QAM orders with different layer counts. The result shows that the 2-layer configuration achieves better BER performance, outperforms the 3-layer result due to less clipping distortion and ILI. Although the 3-layer structure provides higher SE, the additional layer introduces more interference and noise, leading to a noticeable deterioration in BER.

The finding highlights a trade-off in LACO-OFDM systems: increasing the layer count improves SE but adversely affects signal reliability. As a result, the 2-layer configuration works better for applications that require low BER and reliable communication, whereas the 3-layer layout is preferable when increasing SE is the main objective.

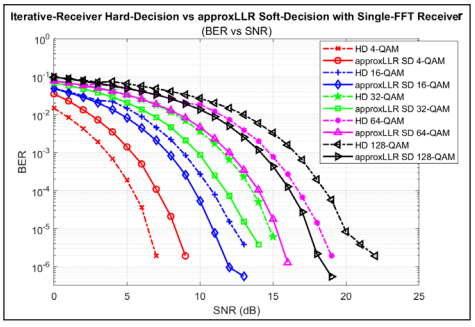

Figure 7. Iterative-receiver HD vs approxLLR SD with single-FFT receiver (different QAM)

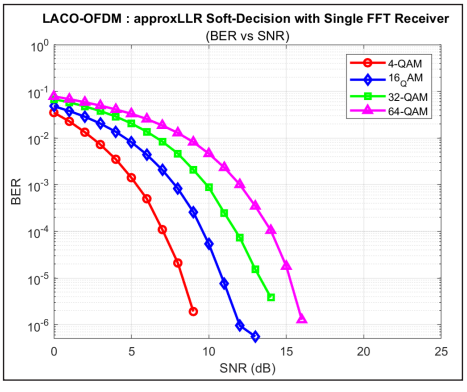

Figure 8. LACO-OFDM approxLLR SD with single-FFT receiver (different QAM)

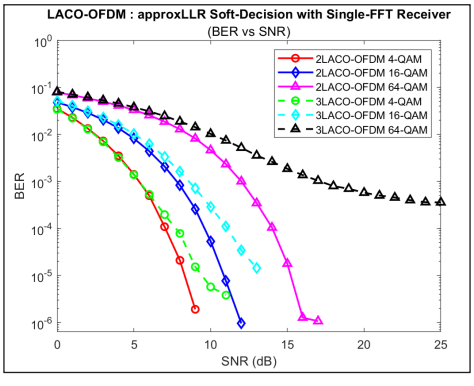

Figure 9. BER performance comparison with different numbers of layers of LACO-OFDM: approxLLR SD with single-FFT receiver

The performance of higher layers in LACO-OFDM is significantly impacted by clipping noise and interference from lower layers. While Layer 1 preserves relatively significant signal power (approximately half of the original due to clipping), higher layers suffer from additional amplitude reduction of superposition, diminishing their contribution to the received signal. Layers 2 and 3 require smaller scaling factors due to weaker amplitudes and higher interference sensitivity, making the conventional 2× scaling factor unsuitable for higher layers.

Under simulation configuration of 10 dB SNR, 30 dBm average received power, and 10% channel attenuation, Figure 10 presents the BER performance for 4-QAM, 16-QAM, and 64-QAM, with optimal scaling factors of 0.7, 0.3, and 0.1 for symbols in higher-layer detection, respectively. The findings show that implementing adaptive scaling factors in higher layers effectively reduces interference and improves BER performance. It contributes a practical trade-off between efficiency and reliability, resulting in a more resilient system.

A comprehensive study was conducted to investigate the relationship between received optical power and energy-per-bit-to-noise density (Eb/No) in a 2-layer LACO-OFDM system employing approxLLR SD demodulation with a single-FFT receiver. The simulation parameters specified in Table 1 were used to analyse the impact of different modulation orders, 4-QAM, 16-QAM, and 32-QAM, on power efficiency and BER performance, with a scaling factor of 0.1 applied to higher layers (layer ≥ 2).

Figure 11 demonstrates a proportional increase in received power with modulation order, indicating reduced noise tolerance in denser constellations. The minimum received powers required for reliable transmission are approximately 0.98 dBm, 7.96 dBm, and 10.98 dBm for 4-QAM, 16-QAM, and 32-QAM at Eb/No = 15dB. Due to the shorter distance between constellation points in higher-order QAM, more received power is required to preserve symbol detection under noisy conditions. The effect becomes more noticeable in OWC systems due to IM/DD constraints (non-negativity signal), which further intensifies the power requirements of higher-order modulation schemes.

Simulation results confirm that the modulation order has a strong influence on both power efficiency and error performance in the proposed approach. While 4-QAM offers excellent noise tolerance and power efficiency, higher-order schemes such as 32-QAM demand significantly more receive power and exhibit higher BER under identical SNR conditions.

Figure 12 demonstrates the received power (in dBm) as a function of Eb/No for a 16-QAM-based LACO-OFDM system under different layer count configurations. As expected, the received power decreases monotonically with increasing Eb/No due to reduced energy demand under improved noise conditions. At Eb/No = 15 dB, the measured received power values are 7.96 dBm (2-layer), 8.05 dBm (3-layer) and 8.08 dBm (4-layer).

These results indicate a slight increase in power consumption as the number of layers increases, attributed to the incremental impact of ILI and clipping noise accumulation. However, the magnitude of difference between the 2-layer and 4-layer systems is limited

to approximately 0.12 dB, indicating that the power overhead introduced by additional layers remains relatively small for moderate modulation orders. This highlights the power efficiency and robustness of the approxLLR SD with a single-FFT receiver scheme in supporting higher-layer configurations without incurring significant energy penalties.

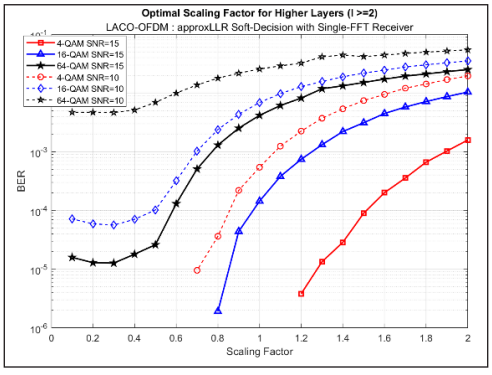

Figure 10. BER versus scale factor on the higher layer of LACO-OFDM approxLLR SD with single-FFT receiver

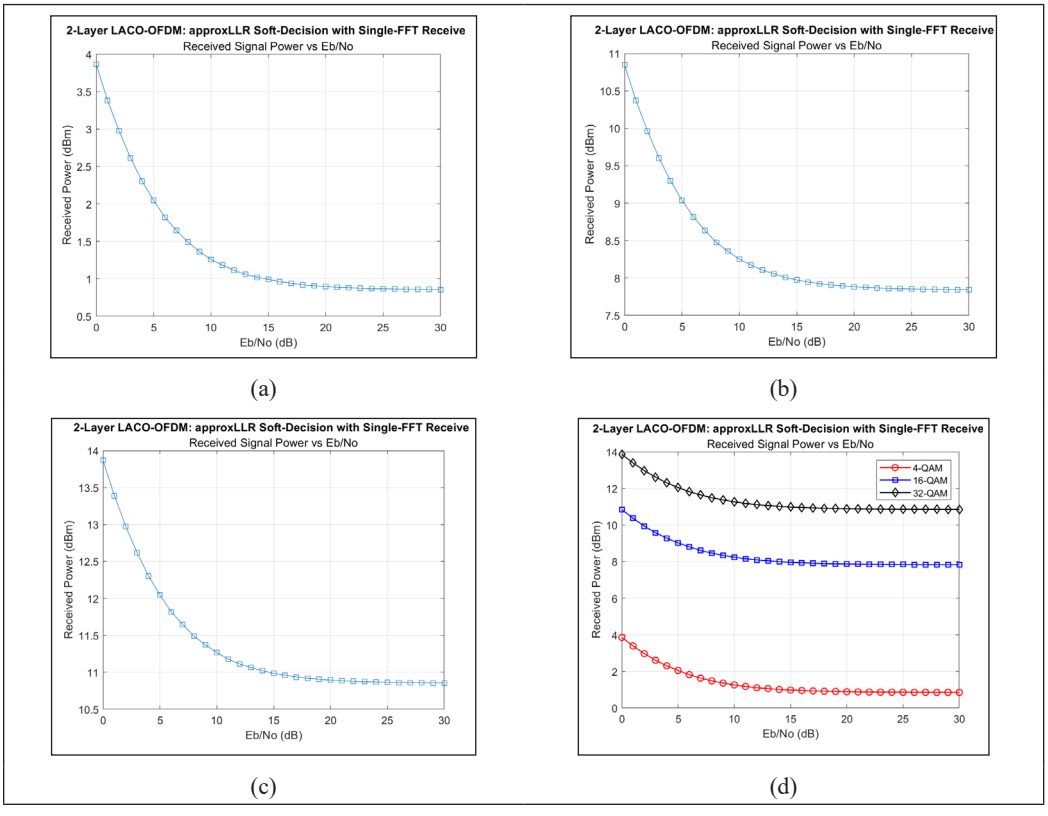

Figure 11. 2-layers of (a) 4-QAM; (b) 16-QAM; (c) 32-QAM; (d) different QAM LACO-OFDM approxLLR SD with single-FFT receiver of BER vs received signal power

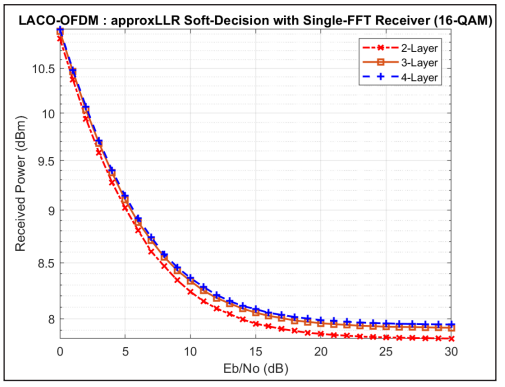

Figure 12. Received power comparison of different numbers of layers, LACO-OFDM approxLLR with 16-QAM

CONCLUSION

The current advancements in various OFDM schemes designed for IM/DD communication have been investigated, and a new theoretical approach of SD demodulation has been derived and validated using MATLAB simulation. The approxLLR SD demodulation has been proposed, integrated with a single-FFT at the receiver module to mitigate the limitation of the conventional LACO-OFDM modulation scheme. The computational bit-wise probabilities for $q = \log_2(M)$ bits, make this SD approach more resilient to channel noise (AWGN) and residual clipping distortion, resulting in a 4 to 5 times performance gain at a target BER of 10^{-4} over the conventional LACO-OFDM iterative-receiver scheme. The incorporation of approxLLR SD demodulation further improves noise-resilience, particularly in higher transmission layers where distortion effects become more pronounced. Enhanced SE is attained through a layered ACO-OFDM structure by enabling layer-by-layer symbol transmission over unused even subcarriers, allowing more effective utilisation of optical bandwidth. With the implementation of single-FFT, which does not require pairwise FFT/IFFT computation to distinguish the frequency-domain of clipping distortion, which makes this proposed approach is relatively simple and the complexity of $\mathcal{O}(N \log_2 N)$, leading to a 2 times reduction of computation can be achieved. Furthermore, the power analysis verifies that the proposed approxLLR SD with single-FFT receiver approach maintains high power and EE, exhibiting only a marginal increase in received power with increasing of layer count.

The performance comparison demonstrates that the proposed LACO-OFDM using approxLLR SD demodulation with a single-FFT receiver consistently outperforms the conventional LACO-OFDM iterative-receiver result while reducing receiver complexity. These results indicate that the proposed approach offers an effective trade-off between performance, SE and implementation simplicity, making it well-suited for VLC system practicality, which requires reliable high data transfer.

ACKNOWLEDGEMENT

The author would like to acknowledge the support from the Fundamental Research Grant Scheme (FRGS) under the grant number of FRGS/1/2022/TK07/UNIMAP/02/82 from the Ministry of Education Malaysia.

DATA AVAILABILITY STATEMENT

The data supporting the findings of this research are accessible upon request from the corresponding author.

CONFLICT OF INTEREST

The authors declare that they have no conflicts of interest related to this work.

LIST OF ABBREVIATIONS

approxLLR	:	Approximate Log-Likelihood Ratio
AWGN	:	Additive white Gaussian noise
BER	:	Bit error rate
CP	:	Cyclic prefix
EE	:	Energy efficiency
FFT	:	Fast Fourier Transform
HD	:	Hard decision
HS	:	Hermitian symmetry
IFFT	:	Inverse Fast Fourier Transform
ILI	:	Inter-layer interference
IM/DD	:	Intensity modulation and direct detection
ISI	:	Inter-symbol interference
LACO-OFDM	:	Layered Asymmetrically Clipped Optical Orthogonal Frequency Division Multiplexing
LLR	:	Log-Likelihood Ratio
MAP	:	Maximum a posteriori
ML	:	Maximum likelihood
M-QAM	:	M-ary quadrature amplitude modulation
OFDM	:	Orthogonal Frequency Division Multiplexing
OWC	:	Optical wireless communication
PS	:	Parallel to serial
QAM	:	Quadrature amplitude modulation
SD	:	Soft decision
SE	:	Spectral efficiency
SNR	:	Signal-to-noise ratio
SP	:	Serial to parallel
VLC	:	Visible light communication

REFERENCES

Aliaberi, A., Sofotasios, P. C., & Muhaidat, S. (2019). Modulation schemes for visible light communications. In *Proceedings of the 2019 International Conference on Advanced Communication Technologies and Networking* (pp. 1-10). IEEE. https://doi.org/10.1109/COMMNET.2019.8742376

Anand, S., Ashish, & Kumar, P. (2024). A low-complexity LLR detector for FrFT-IM-OFDM in the presence of ICI. In *Proceedings of the 2024 27th International Symposium on Wireless Personal Multimedia Communications* (pp. 1-5). IEEE. https://doi.org/10.1109/WPMC63271.2024.10863056

Azim, A. W., Le Guennec, Y., Chafii, M., & Ros, L. (2021). LACO-OFDM with index modulation for optical wireless systems. *IEEE Wireless Communications Letters, 10*(3), 664-667. https://doi.org/10.1109/LWC.2020.3045119

Bai, R., Hranilovic, S., & Wang, Z. (2022). Low-complexity layered ACO-OFDM for power-efficient visible light communications. *IEEE Transactions on Green Communications and Networking, 6*(3), 1780-1792. https://doi.org/10.1109/TGCN.2022.3147970

Cao, X., Liu, Y., & Hu, D. (2019). Simplified LLR algorithm for M-QAM demodulation. *The Journal of Engineering, 2019*(21), 7370-7375. https://doi.org/10.1049/joe.2019.0634

Hu, Z., Chen, F., Wen, M., Ji, F., & Yu, H. (2018). Low-complexity LLR calculation for OFDM with index modulation. *IEEE Wireless Communications Letters, 7*(4), 618-621. https://doi.org/10.1109/LWC.2018.2802949

Hussein, Y. M., Mutlag, A. H., & Al-Nedawe, B. M. (2021). Comparisons of soft decision decoding algorithms based on an LDPC wireless communication system. *IOP Conference Series: Materials Science and Engineering, 1105*(1), Article 012039. https://doi.org/10.1088/1757-899X/1105/1/012039

Jativa, P. P., Azurdia-Meza, C. A., Canizares, M. R., Zabala-Blanco, D., & Montejo-Sanchez, S. (2020). Performance analysis of OFDM-based VLC schemes in NLOS channels. In *Proceedings of the 2020 South American Colloquium on Visible Light Communications* (pp. 1-6). IEEE. https://doi.org/10.1109/SACVLC50805.2020.9129862

Li, J., Liu, X., Ren, Y., & Huang, Z. (2021). Single-FFT receiver with pairwise maximum likelihood for layered ACO-OFDM. *IEEE Photonics Journal, 13*(4), 1-6. https://doi.org/10.1109/JPHOT.2021.3105812

Liu, G., Peng, M., Liu, C., Chen, M., Zhou, H., & Chen, Q. (2018). Receiver sensitivity improvement of a layered ACO-OFDM system enabled by layered-DFT/OCT precoding technique. In *Proceedings of the 2018 Asia Communications and Photonics Conference* (pp. 1-3). IEEE. https://doi.org/10.1109/ACP.2018.8595736

Liu, X., Li, J., Li, J., & Huang, Z. (2020). Analysis of the single-FFT receiver for layered ACO-OFDM in visible light communications. *Journal of Lightwave Technology, 38*(17), 4757-4764. https://doi.org/10.1109/JLT.2020.2994633

Lowery, A. J. (2020). Spectrally efficient optical orthogonal frequency division multiplexing. *Philosophical Transactions of the Royal Society A: Mathematical, Physical and Engineering Sciences, 378*(2169), Article 20190180. https://doi.org/10.1098/rsta.2019.0180

Mao, D., Chen, C., & Bai, B. (2020). An improved simplified soft demodulation algorithm for 64QAM signal. In *Proceedings of the 2020 IEEE 3rd International Conference on Electronic Information and Communication Technology* (pp. 157-160). IEEE. https://doi.org/10.1109/ICEICT51264.2020.9334307

Nakano, H., Tamura, K., Ueno, H., Takemoto, R., Cha, J., & Ahn, C. (2023). Each layer adaptation for throughput enhancement of LACO-OFDM. In *Proceedings of the 2023 International Conference on Advanced Technologies for Communications* (pp. 202-206). IEEE. https://doi.org/10.1109/ATC58710.2023.10318938

Olivatto, V. B., Lopes, R. R., & de Lima, E. R. (2017). Simplified method for log-likelihood ratio approximation in high-order modulations based on the Voronoi decomposition. *IEEE Transactions on Broadcasting, 63*(3), 583-589. https://doi.org/10.1109/TBC.2017.2704424

Othman, N., Beson, M. R., Aljunid, S. A., & Endut, R. (2024). Review: Outdoor visible light communication on modulation and receiver denoising scheme. *AIP Conference Proceedings, 3050*(1), Article 030038. https://doi.org/10.1063/5.0195503

Seow, Y. L., Rashidi, C. B., Aljunid, S. A., Ali, N., & Endut, R. (2021). 20 Mb/s experimental demonstration using modulated 460 nm blue LED for underwater wireless optical communications (UOWC). *Journal of Physics: Conference Series, 1878*(1), Article 012069. https://doi.org/10.1088/1742-6596/1878/1/012069

Vappangi, S., Mani, V. V., & Sellathurai, M. (2021). *Visible light communication: A comprehensive theory and applications with MATLAB®*. CRC Press.

Wang, C., Wang, X., Jiang, K., & Zou, J. (2023). Viterbi soft demodulation algorithm for CPFSK systems. In *Proceedings of the 2023 8th International Conference on Communication, Image and Signal Processing* (pp. 522-527). IEEE. https://doi.org/10.1109/CCISP59915.2023.10355684

Wang, Q., Qian, C., Guo, X., Wang, Z., Cunningham, D. G., & White, I. H. (2015). Layered ACO-OFDM for intensity-modulated direct detection optical wireless transmission. *Optics Express, 23*(9), 12382-12393. https://doi.org/10.1364/OE.23.012382

Yan, X., He, J., Shi, J., Zhou, Z., & Tang, Q. (2020). Time-efficient adaptive modulation scheme for LACO-OFDM in VLC systems. *Optics Communications, 474*, Article 126069. https://doi.org/10.1016/j.optcom.2020.126069

Zhang, C., Baharudin, M. A., Guo, T., Wang, J., & Jia, Z. (2025). A survey on the latest developments of OFDM schemes for optimising the capacity and reliability of visible light communication (VLC) systems. *KSII Transactions on Internet and Information Systems, 19*(5), 1625-1647. https://doi.org/10.3837/tiis.2025.05.012

Zhang, T., Sun, L., Zhao, C., Qiao, S., & Ghassemlooy, Z. (2021). Low-complexity receiver for HACO-OFDM in optical wireless communications. *IEEE Wireless Communications Letters, 10*(3), 572-575. https://doi.org/10.1109/LWC.2020.3038181

Zhang, X., Babar, Z., Zhang, R., Chen, S., & Hanzo, L. (2019). Multi-class coded layered asymmetrically clipped optical OFDM. *IEEE Transactions on Communications, 67*(1), 578-589. https://doi.org/10.1109/TCOMM.2018.2869821

Zhang, X., Chen, S., & Hanzo, L. (2020). On the discrete-input continuous-output memoryless channel capacity of layered ACO-OFDM. *Journal of Lightwave Technology, 38*(18), 4955-4968. https://doi.org/10.1109/JLT.2020.2996541

Zhang, X., Wang, Q., Zhang, R., Chen, S., & Hanzo, L. (2017). Performance analysis of layered ACO-OFDM. *IEEE Access, 5*, 18366-18381. https://doi.org/10.1109/ACCESS.2017.2748057